Submitted to *J. Phys. Chem. A* on 23 June, 2022

Together, not separately, OH and O_3 oxidize $Hg^{(0)}$ to $Hg^{(II)}$ in the atmosphere

Pedro J. Castro[1], Vladimir Kellö[2], Ivan Cernušák[2] and Theodore S. Dibble[1,*]

[1] Department of Chemistry, State University of New York College of Environmental Science and Forestry, 1 Forestry Drive, Syracuse, New York 13210, United States

[2] Department of Physical and Theoretical Chemistry, Faculty of Natural Sciences, Comenius University in Bratislava, 84215 Bratislava, Slovakia

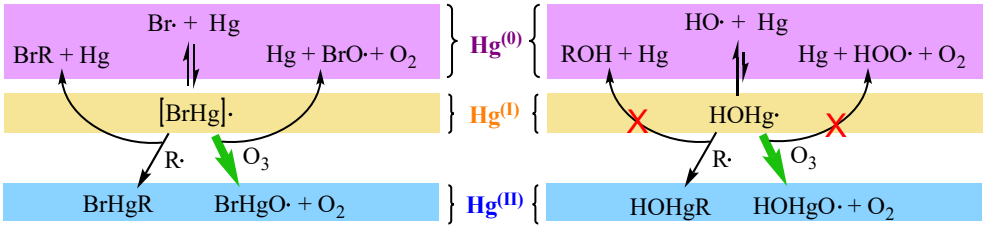

ABSTRACT

Mercury, a highly toxic metal, is emitted to the atmosphere mostly as gaseous $Hg^{(0)}$. Atmospheric $Hg^{(0)}$ enters ecosystems largely through via uptake by vegetation, while $Hg^{(II)}$ largely enters ecosystems in oceans and via rainfall. Consequently, the redox chemistry of atmospheric mercury strongly influences its fate and its global biogeochemical cycling. Here we report on the oxidation and reduction of $Hg^{(I)}$ (BrHg and HOHg radicals) in reactions with ozone, and how the electronic structure of these $Hg^{(I)}$ species affects the kinetics of these reactions. The oxidation reactions lead to XHgO• + O_2 (X=Br and OH), while the reduction reaction produces $Hg^{(0)}$, HOX, and O_2. According to our calculations with CCSD(T), NEVPT2, and CAM-B3LYP-D3BJ, the kinetics of both oxidation reactions are very similar. These two oxidation reactions are much faster than their reduction counterparts, and this effect is remarkably stronger for the oxidation of $HOHg^{(I)}$ by ozone. Modeling of field data supports the idea that OH and/or O_3 (rather than Br) dominates $Hg^{(II)}$ production in the continental boundary layer. Almost all models invoking OH- and ozone-initiated oxidation of $Hg^{(0)}$ assume that these reactions directly produces $Hg^{(II)}$, despite the lack of plausible mechanism for these oxidation reactions. The present work helps reconcile modeling results with mechanistic insights.

1. INTRODUCTION

Mercury is well-known as one of the most toxic metals for vertebrates.[1,2] It can be released to the environment from both natural and anthropogenic sources,[3,4] and also from reemissions of previously deposited mercury.[5,6] Mercury is a global pollutant because of its ability to travel through the atmosphere far from emission sources.[7,8] Despite that the atmosphere only contain ~0.3% of the total environmental mercury,[9] it remains crucial for the mercury cycle because gas-phase mercury redox chemistry[10-18] greatly influences when and where mercury deposits to ecosystems (Figure 1).[19-23] Specifically, $Hg^{(II)}$ readily deposits to lakes and oceans, while $Hg^{(0)}$ is much more likely to be taken up in vegetation.[6,9,23]

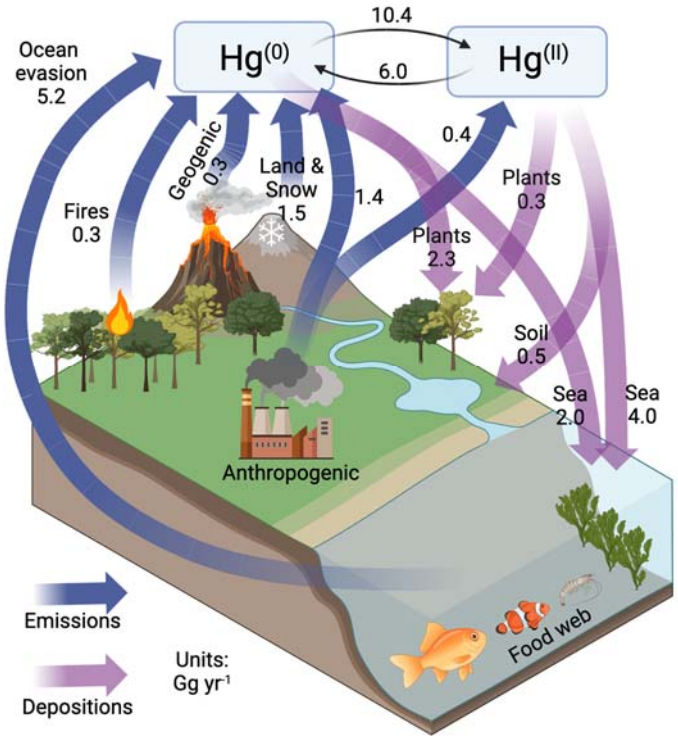

Figure 1. Mercury cycle based on References 23 and 55. The deposition labeled as soil includes land and snow.

Once mercury is deposited, it can be bioaccumulated, biomagnified and transported in the form of organomercury, especially through the aquatic food chain, and ultimately have negative effects on human and animal health.[24-30] Therefore, mercury is a serious hazard that has been a major concern amongst environmental and scientists for decades. Despite great strides in our understanding of the mechanisms of mercury chemistry in the atmosphere, the lack of knowledge of the kinetics

prevents accurate prediction of mercury transport. In fact, recent advances in our understanding have led to situations in which models alternately yield far too much mercury oxidation or far too much reduction to be reconciled with observations. This limits the utility of atmospheric models in contributing to understanding biogeochemical cycling of mercury.[6,11,31]

Although some experiments suggest that $Hg^{(0)}$ reacts with O_3 at an appreciable rate,[32-35] it has long been argued that the observed reaction rates do not correspond to those for a gas phase $Hg^{(0)} + O_3$ reaction.[4,36,37] In contrast, oxidation of $Hg^{(0)}$ to $Hg^{(I)}$ is assumed to occur mainly by reaction with atomic Br (R1). This reaction with Br is assumed to globally dominate Hg oxidation in comparison with oxidation by other halogens, such as Cl and I,[10,38] given the higher concentration of Br and the strength of the bond of the radicals to $Hg^{(0)}$.[39-45] Several experiments have measured the rate constant for the oxidation of $Hg^{(0)}$ initiated by Br,[34,46,47,48] which is a barrierless and exothermic reaction leading to $BrHg^{(I)}$.[11,12,39,49] Despite that $BrHg^{(I)}$ can dissociate back to $Hg^{(0)}$, the oxidation reactions by addition of radicals (R2)[12,18] seem to be faster under atmospheric conditions.[19,] $BrHg^{(I)}$ can also be reduced to $Hg^{(0)}$ when radicals, R• (R• = NO, NO_2, and Br), displace the Hg from the Br atom (R3).[18,49,51,52] This chemistry can be summarized by reactions R1-R3:

$$Hg^{(0)} + Br \rightarrow BrHg^{(I)} \quad \text{(R1)}$$

$$BrHg^{(I)} + R\bullet \rightarrow BrHg^{(II)}R \quad \text{(R2)}$$

$$BrHg^{(I)} + R\bullet \rightarrow Hg^{(0)} + BrR \quad \text{(R3)}$$

The OH radical can mimic Br in reaction with $Hg^{(0)}$ to analogously produce $HOHg^{(I)}$ (R4) in barrierless and exothermic reaction,[37,53,54] but its atmospheric relevance has been questioned because of the low stability of $HOHg^{(I)}$.[12,19,56] $HOHg^{(I)}$, like $BrHg^{(I)}$, can form stable $Hg^{(II)}$ species by reacting with radicals such as NO_2 or HOO (R5),[19] but there is no evidence of displacement of Hg atom by radicals leading to reduction reactions (R6).

$$Hg^{(0)} + OH \rightarrow HOHg^{(I)} \quad \text{(R4)}$$

$$HOHg^{(I)} + R\bullet \rightarrow HOHg^{(II)}R \quad \text{(R5)}$$

$$HOHg^{(I)} + R\bullet \rightarrow Hg^{(0)} + HOR \quad \text{(R6)}$$

When considering the fate of radicals, an atmospheric chemist will naturally consider reaction with ozone, on account of its abundance in the atmosphere and its propensity for reacting with radicals. Lam[57] was the first to propose the importance of ozone in oxidizing $BrHg^{(I)}$ to $Hg^{(II)}$, via :

$$BrHg^{(I)} + O_3 \rightarrow BrHg^{(II)}O + O_2 \quad \text{(R7)}$$

A global modeling effort by Saiz-Lopez et al.[6] included R7 in one of their model runs with a rate constant, k_7, of 1.0×10^{-10} cm^3 $molec^{-1}$ s^{-1}. This rate constant was estimated based on the absence of a barrier to R7 in their density functional theory (DFT) results. Saiz-Lopez et al. did not consider the analogous reaction of $HOHg^{(I)}$:

$$HOHg^{(I)} + O_3 \rightarrow HOHg^{(II)}O + O_2 \quad \text{(R8)}$$

Shah et al. included R7 and R8 in the GEOS-Chem global model using $k_7 = k_8 = 3.0 \times 10^{-11}$ cm^3 $molec^{-1}$ s^{-1}.[55] Their value of k_7 was supported by preliminary experimental work and computations (at DFT and CASPT2) showing that R7 was barrierless. The assumption of similar rate constants for reactions of $HOHg^{(I)}$ and $BrHg^{(I)}$ is supported by the similarity of the thermodynamics and activation barriers of their reactions and exothermicity of their barrierless reactions.[19] Very recently, Gomez Martin et al. carried out the first determination of the rate constant of R7 using laser-flash photolysis with laser-induced fluorescence: $7.5 \pm 0.6 \times 10^{-11}$ cm^3 $molec^{-1}$ s^{-1} (at 295 K).[58] They assumed the reaction proceeded via R7.

According Shah et al.,[55] ozone is the primary oxidant of $Hg^{(I)}$ to $Hg^{(II)}$. Photolysis and thermal decomposition of $BrHg^{(I)}$ are much slower than its reaction with ozone, so the main fate of $BrHg^{(I)}$ is oxidation. A previous modeling study that did not include R8 had found that $HOHg^{(I)}$ mostly dissociated, and that OH-initiated oxidation of $Hg^{(I)}$ contributed <1% of global $Hg^{(0)}$ oxidation.[19] The inclusion of R8 (with $k = 3.0 \times 10^{-11}$ cm^3 $molec^{-1}$ s^{-1}) enabled OH-initiated oxidation to contribute one-third of the global $Hg^{(II)}$ production.[55] Only the reaction of $HOHg^{(I)}$ with O_3 is sufficiently fast to enable $HOHg^{(I)}$ to contribute significantly to global $Hg^{(II)}$ production.

In this study, we use computational chemistry to determine the kinetics of oxidation of $HOHg^{(I)}$ by O_3 (R8) and compare the kinetics of R8 with the analogous reaction of $BrHg^{(I)}$ (R7). The

comparison to R7 holds particular value in light of two facts: the recent experimental determination of $k_7(295\ K)$[58] and the complete absence of experimental data on gas-phase $HOHg^{(I)}$. In addition, we also study the reduction of $YHg^{(I)}$ to $Hg^{(0)}$ by ozone:

$$BrHg^{(I)} + O_3 \rightarrow Hg^{(0)} + BrO + O_2 \quad (R9)$$

$$HOHg^{(I)} + O_3 \rightarrow Hg^{(0)} + HOO + O_2 \quad (R10)$$

including how the thermodynamics and kinetics are affected by the electronic structure of the two $Hg^{(I)}$ species.

The main objective of this work is to shed light about the role of O_3 in the redox chemistry of Hg in the atmosphere. Although there is no chemically or physically plausible mechanism for O_3 to directly oxidize $Hg^{(0)}$ to $Hg^{(II)}$, the oxidation of $HOHg^{(I)}$ by O_3 to $HOHg^{(II)}O$ would enable OH-initiated oxidation to contribute significantly to GEM oxidation. In this manner, OH and O_3, together, but not separately, could oxidize GEM to GOM. Demonstrating the feasibility of this mechanism for GEM oxidation would help resolve the discrepancy between modeling that requires OH and/or O_3 to explain observations of GOM[59-62] abundance at low [Br] (especially in the continental boundary layer) *versus* the prior study of Dibble et al. that provided strong physical arguments against this possibility.[19]

COMPUTATIONAL DETAILS

Most the calculations presented in this article were carried out in ORCA program 5.0.1[63] and Gaussian 16[64] using a combination of Dunning's augmented correlation consistent triple-zeta basis sets: aug-cc-pVTZ[65,66] and aug-cc-pVTZ-PP[67] basis sets. The first one was used for oxygen and nitrogen atoms, while aug-cc-pVTZ-PP for the Br and Hg atoms.[68,69] The aug-cc-pVTZ-PP basis set was used in combination with the Stuttgart-Koln small-core multiconfiguration-Dirac-Hartree-Fock-adjusted (SK-MCDHF-RSC) effective core potentials (ECP) via energy-consistent pseudopotentials (PP) for the 60 innermost electrons of Hg (ECP60MDF) and the 10 innermost electrons of Br (ECP10MDF). This combination takes into account the relativistic effects on the electronic energies, while the orbitals out of the pseudopotential are described similar to the aug-cc-pVTZ basis set. This combination of basis sets is denoted below as AVTZ. The Frozen-Core approximation was applied to the first 8 and 18 explicitly treated electrons of Hg and Br,

respectively, in most of the Post-Hartree-Fock calculations. Preliminary calculations were carried out by optimizing at MP2,[70] B97D3,[71,72] BLYP[73,74] and CAS(7,6),[75] followed by single point energies at CASPT2,[76,77] NEVPT2,[78,82] AQMRCC,[83] CR-CC(2,3)[84] and MRCI+Q (Figures S1 to S5 in Supp. Information).[85,86]

In addition, for the reaction $HOHg^{(I)}$ + O_3 we have performed a 3D potential surface scan at CASPT2 level in MOLCAS.[87] Scalar relativistic DK2[88,89]-CASPT2/ANO-RCC-VDZP[90,91] computations utilized 13 electrons in 11 orbitals (Figure S6 in Supp. Information) that cover both the O-O bond breaking and Hg-O bond formation. We mapped the PES with respect to two coordinates: d_{HgO} (Hg-O_3 distance) – bond formation during the terminal oxygen migration from O_3 to HOHg and d_{OO} (O-O_2 distance) – bond breaking between terminal and central oxygen in O_3 (see Figure S7 in Supp. Information). These exploratory calculations served as a guide in the subsequent detailed study of the $HOHg^{(I)}$ + O_3 reaction profiles.

To study the energy profiles for such reactions it is necessary to have a good description of the intermolecular interactions at long distances. Dispersion corrected and/or long-range corrected functionals provide good accuracy at longer distances at low computational cost. Therefore, we have selected CAM-B3LYP[92,93] as our main functional, in combination with the D3BJ[94,95] empirical dispersion correction. Once the reactants and products were fully optimized at CAM-B3LYP-D3BJ, we used the same functional to study the topography of the potential energy surfaces (PES) of the ground state along the reaction coordinates by relaxed scans along the distances between a terminal oxygen atom of O_3 and the Br, Hg or HO of $BrHg^{(I)}$ or $HOHg^{(I)}$, depending on the reaction to be studied. For example, in the oxidation of $BrHg^{(I)}$ and $HOHg^{(I)}$, d_{HgO} (Hg-O_3 distances) were scanned, but for the reduction reactions, the d_{BrO} (Br-O_3 distance) and d_{HOO} (HO-O_3 distance) were scanned, respectively. To study the stability of exit-channel complexes ($YHg^{(II)}O$--O_2), we scanned d_{OO} (O-O_2 distance) starting from the geometries of the exit-channel complexes.

The scans were carried out after obtaining the most stable wavefunctions within the unrestricted approach. Then, we used the correlated coupled cluster singles and doubles with perturbative triples (CCSD(T))[96,97] method to obtain energies at points along scans. In addition, strongly contracted *N*-electron valence state second-order perturbation theory (SC-NEVPT2)[78-82] was used to take into account the dynamic electron correlation. The complete active space (CAS)[75] SCF method was used to generate the reference wavefunctions as a full configuration interaction

expansion in the selected active spaces. Figure 2 illustrates the active spaces for the reactants. The active space to study the energy profiles for the reactions between $BrHg^{(I)}$ and O_3 is CAS(19,14). Following the same reasoning, the active spaces for the reactions between $HOHg^{(I)}$ and O_3 are CAS(17,13). The configuration spaces for $YHg^{(I)}$ + O_3 are formed by 168,168 and 87,802 configurations for Y = Br and OH, respectively.

Active Space O_3: CAS(12,9)

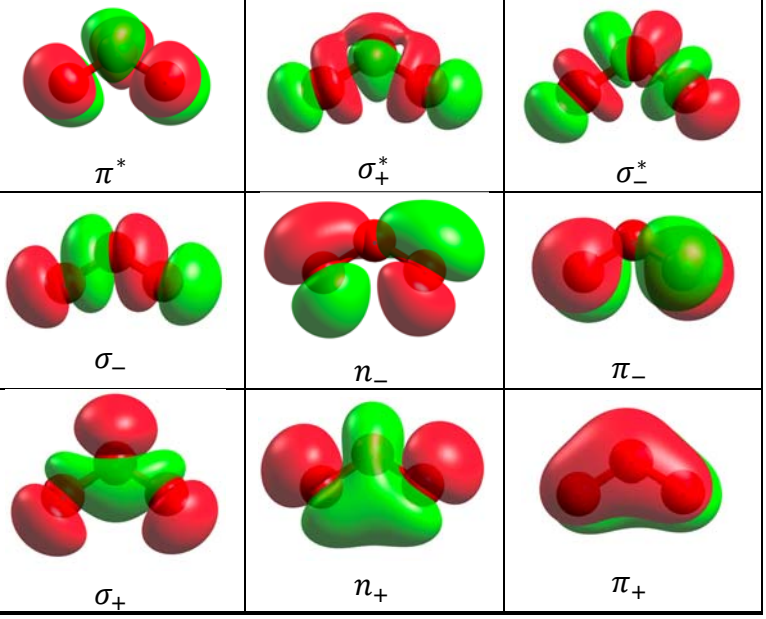

Active Space BrHg: CAS(7,5)

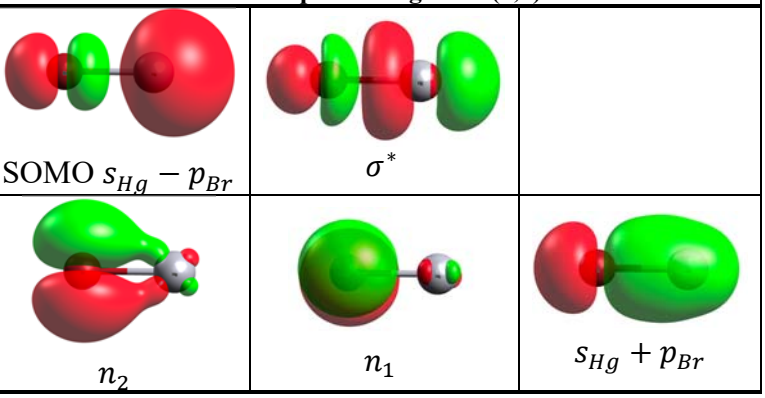

Active Space HOHg: CAS(5,4)

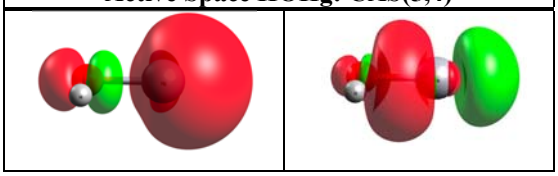

SOMO $s_{Hg} - p_O$	σ^*
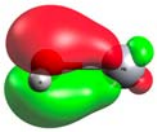	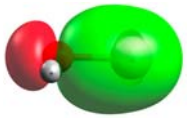
n	$s_{Hg} + p_O$

Figure 2. Molecular orbitals of $BrHg^{(I)}$, $HOHg^{(I)}$ and O_3 included in the active spaces used for the reference wavefunctions.

In order to get zero-point energy (ZPE) and Gibbs free Energies corrections ($G_{corr}(T)$), frequency calculations were performed at CAM-B3LYP-D3BJ level at each point along the scans. Then, the free energy (G) along each point of the paths were calculated by adding $G_{corr}(T)$ to the energy (E_{elec}) from CCSD(T) and NEVPT2. This was used to determine the position of the variational TS at temperatures of 200, 220, 240, 260, 280, 298.15, 300, 320, 340, and 360 K. The minimum value of the canonical transition state theory (CTST) rate constant, $k_{CTST}(T)$, along the path corresponds to the variational TST rate constant, $k_{VTST}(T)$. The relative energies, vibrational frequencies, and rotational constants from these points were used as input for the thermo program (from the MultiWell Program Suite[98-100]) to compute the rate constants at each temperature with CTST.

RESULTS AND DISCUSSION

According to the CCSD(T) and CASSCF calculations we previously reported, the $BrHg^{(I)}$ radical (doublet) possesses a delocalized unpaired electron that distributes comparable spin-density on the Br atom as on the Hg atoms (Figure 3). This explains why $BrHg^{(I)}$ can react with radicals, R•, such as Br, NO, NO_2, without a barrier to form $Hg^{(0)}$ + BrR (R3).[18,49,51] It seems that the products of $BrHg^{(I)}$ reactions should strongly depend on the orientation of the molecular collisions with other radicals or species such as O_3. If the collision occurs between Hg atom and another radical center, the reaction can readily form $Hg^{(II)}$; however, when the collision rather involves the Br atom, the reduction reaction to $Hg^{(0)}$ takes place. In contrast to $BrHg^{(I)}$, the spin-density of $HOHg^{(I)}$ is mostly localized on the Hg atom (Figure 3). Therefore, we hypothesized that, unlike $BrHg^{(I)}$ which leads to mercury oxidation or reduction by reacting with radicals or O_3, $HOHg^{(I)}$ will react with radicals almost exclusively by oxidation pathways toward $Hg^{(II)}$.

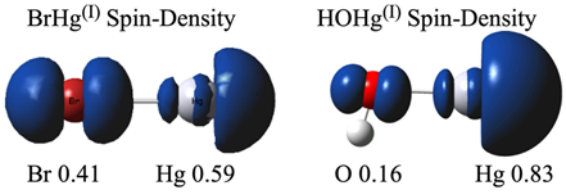

Figure 3. Spin-density based on Mulliken population analysis using linearized density from CCSD(T). The spin-densities were confirmed by the Orbital-Optimized Coupled-Cluster Doubles (OOCCD) method.

Overview of the Oxidation of $YHg^{(I)}$

Given the symmetry of the O_3, the oxidation reaction of $YHg^{(I)}$ can be triggered by two equivalent barrierless pathways characterized by the collision of any of the two end-oxygens of the O_3 with the Hg atom of $YHg^{(I)}$. At long distances, the orientation of O_3 is not relevant, but as the two molecules get closer, the preferred orientation for Hg oxidation creates a bonding interaction from the overlap of the portion of the SOMO of $YHg^{(I)}$ located on Hg with the π system of O_3 (Figure 2). The fully-formed bond yields to the $Hg^{(II)}$ species YHgOOO which acquires a planar structure that is the global energy minimum of the PES. The other equivalent reaction pathway also has a minimum, which is nearby, creating a double well region whose TS is easily accessible. Each minimum of the double well is an exit-channel complex, which can dissociate to $YHg^{(II)}O$ and O_2 by breaking the weak $YHg^{(II)}O$-O_2 bond (analogous to HO_3).[101,102]

Oxidation of $BrHg^{(I)}$ by O_3

Relaxed scans were performed at CASSCF level; however, the topography of the PES was characterized by a barrier imposed by a transition state (TS) formed by an avoided crossing between the ground and an excited state. This barrier disappears as dynamic electron correlation is added (Figure S1 in Supp. Information). Given that the calculations of $k(T)$ depend on the normal modes along the reaction path, the CASSCF frequencies do not properly represent the shape of the PES. Since numerical NEVPT2 optimizations are computationally prohibited, we adopted the strategy of combining DFT values of $G_{corr}(T)$ with NEVPT2 electronic energies in order to locate the variational TS. The energy profiles at CAM-B3LYP-D3BJ and BLYP level show a barrierless potential energy surface along the reaction coordinate, whose minimum is a final complex (FC)

that is expected to be vibrationally excited and should rapidly dissociate to $BrHg^{(II)}O$ and O_2 (Figure S2 in Supp. Information). The topography of the PES along d_{HgO} matches very well at NEVPT2, CAM-B3LYP-D3BJ, ωB97X-D3BJ and CCSD(T) level. On the other hand, the PES obtained at BLYP and B97D3 are similar to each other, however, unlike the other methods used, these functionals show a much wider "parabola" around the minimum, leading to significant interaction at large inter-reactant distances (green line in Figure S2 in Supp. Information). Since CAM-B3LYP-D3BJ yielded a potential energy profile that most resembled the CCSD(T) and NEVPT2 profiles, we report results based on scan points and vibrational frequencies obtained at CAM-B3LYP-D3BJ level.

Despite that the T1 diagnostic shows an important multiconfigurational character (maximum of 0.039) along the whole reaction path (Figure S3 in Supp. Information), the topography of the PES match very well with NEVPT2 and CAM-B3LYP-D3BJ, with the exception of one point with d_{HgO} = 2.742 Å. Luckily, this inconsistency does not affect the calculation of the reaction rate constant. The reaction coordinate is mostly defined by the d_{HgO} and d_{OO} distances. The d_{HgO} dominates the reaction that forms the final complex ($BrHg^{(II)}O$--O_2) from $BrHg^{(I)}$ and O_3. The d_{OO} distance dominates the formation of separate products ($BrHg^{(II)}O$ and O_2) from $BrHg^{(II)}O$--O_2. This complex is 48.8 and 42.7 kcal mol^{-1} lower than reactants according to the ZPE-corrected CCSD(T) and NEVPT2 energies, respectively. Since BrHgOOO is planar, the two equivalent approaches of ozone to the Hg atom lead to superimposable mirror image structures of BrHgOOO, that is, one and the same molecule. The TS separating the two equivalent minima belong to C_{2v} point group ($TS_{min\text{-}min}$) and it is only 2.4 kcal mol^{-1} higher that the exit-channel complexes at NEVPT2 (Figure 4).

The maximum energy along the Gibbs free energy profiles increase as the temperature increases. Figure 4 shows ΔG from 200 to 360 K in intervals of 40 K, and the free energy barriers ($\Delta G^{\ddagger}$) goes from 4.0 to 9.0 kcal mol^{-1} at CCSD(T) level as the temperature increases from 200 to 360 K. The range of barriers obtained with CAM-B3LYP-D3BJ is 4.2 – 9.1 kcal mol^{-1} which match very well with CCSD(T), however, NEVPT2 show higher barriers ranging from 5.2 to 10.1 kcal mol^{-1}. The variational TS is displaced to slightly shorter d_{HgO} when the temperature increases (Figure 5).

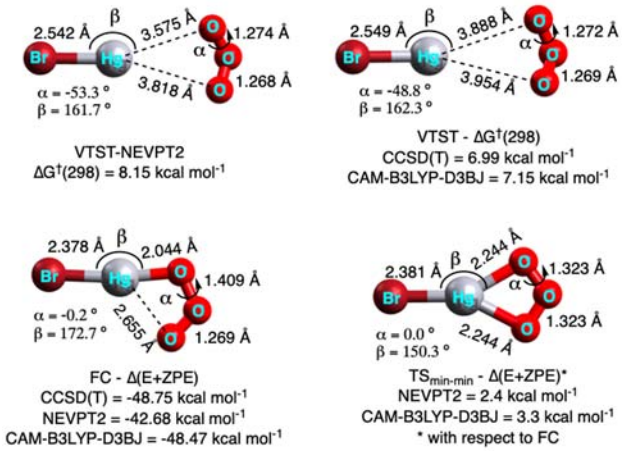

Figure 4. Variational TS, $TS_{min\text{-}min}$ and FC geometries for R7 ($BrHg^{(I)} + O_3 \rightarrow BrHg^{(II)}O + O_2$). Energies (in kcal mol^{-1}) at CCSD(T), NEVPT2, and CAM-B3LYP-D3BJ.

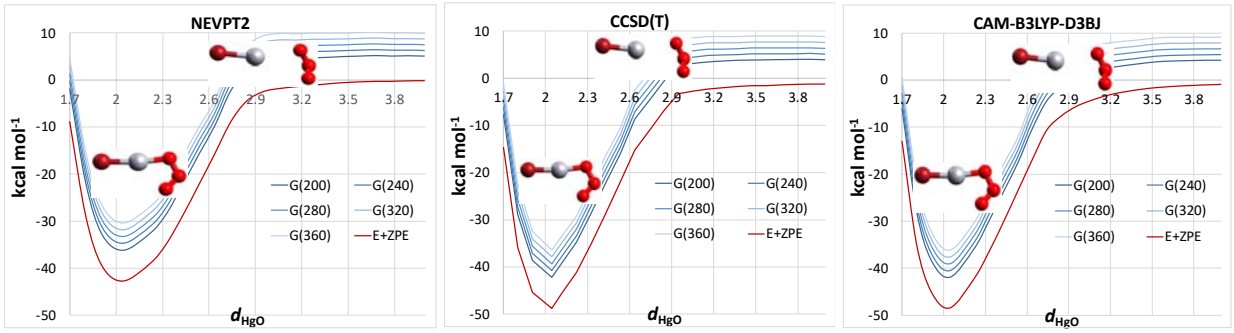

Figure 5. Energy profiles (kcal mol^{-1}) including ZPE along the d_{HgO} distance. Energies have been calculated using NEVPT2, CCSD(T) and CAM-B3LYP-D3BJ, taking as a reference the reactants optimized at CAM-B3LYP-D3BJ and separated at infinite distance, excepting the NEVPT2 profile that took as a reference energy a d_{HgO} = 4.20 Å. $G(T) = E_{elec}^{High\text{-}Level} + G_{corr}^{DFT}(T)$; $E = E_{elec}^{High\text{-}Level} + ZPE^{DFT}$.

Three sets of temperature dependent rate constants were calculated for the oxidation of $BrHg^{(I)}$ by O_3 (R7) in MultiWell (Table S1): the first set was obtained by using as input the rotational constants, vibrational frequencies and thermochemistry for reactants calculated at CCSD(T), and the rotational constants and vibrational frequencies of the variational TS calculated at CAM-B3LYP-D3BJ level. The second set of rate constants uses the same data as the first one, but replacing the relative energies by the ones obtained at NEVPT2. The third set has been calculated

only using data from CAM-B3LYP-D3BJ. Our CAM-B3LYP-D3BJ and CCSD(T) rate constants at 298 K (6.5 and 8.7 × 10^{-11} cm^3 $molec^{-1}$ s^{-1}) bracket the experimental value of 7.5 ± 0.6 × 10^{-11} cm^3 $molec^{-1}$ s^{-1} (at 295 K).[58] The rate constants computed at CAM-B3LYP-D3BJ and CCSD(T) are nearly temperature independent (Figure 6). They vary by only ~20% over the range 200 K ≤ T ≤ 360 K. The NEVPT2 rate constant at 298 K is a factor of 14 lower than the experimental value, and increases monotonically with increasing temperature by a factor of 2.4 over the same temperature range.

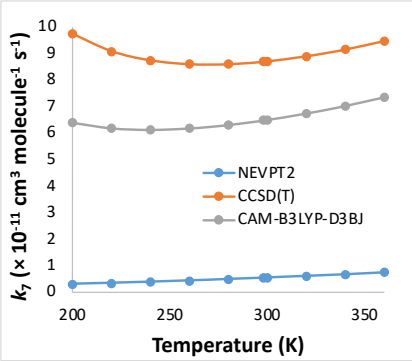

Figure 6. Variational TST rate constant k_7(T) (× 10^{-11} cm^3 $molecule^{-1}$ s^{-1}) for $BrHg^{(I)}$ oxidation as a function of the temperature according to CCSD(T), NEVPT2 and CAM-B3LYP-D3BJ energies.

Once the system overcomes the free energy barrier, the FC is formed (Figure 5). Unlike the variational TSs, this exit-channel complex is planar and it is 6.69, 6.81 and 4.64 kcal mol^{-1} lower than the final products (BrHgO and O_2) when calculated at CCSD(T), NEVPT2 and CAM-B3LYP-D3BJ, respectively. The FC is characterized has a weak O-O bond (d_{OO} = 1.409 Å) that is much shorter than that in HOOH (1.475 Å)[103] or the HO-OO bond distance (1.688 Å).[104] According to CAM-B3LYP-D3BJ, the cleavage of the O-O bond takes place through a TS that is 8.9 kcal mol^{-1} higher than FC. This barrier should be easily overcome by the 48 kcal mol^{-1} of kinetic energy deposited into BrHgOOO by the reaction. Note that calculations on HO--O_2 bond cleavage were beset by artificial barriers above the bond energy.[101,102,105]

Oxidation of HOHg by O_3

The 3D scan of potential energy surface calculated at the DK-CASPT2/ANO-RCC-VDZP level is displayed in Figure 7. It indicates that there is either very small or no barrier for the oxygen migration from O_3 to $HOHg^{(I)}$. At the entry channel, the geometry of ozone changes only very slightly ($R(O_4\text{-}O_5)$ being almost constant), after reaching $R(Hg\text{-}O_4)$ value around 2.5-2.6 Å, one can observe a quick migration of O_4 towards $HOHg^{(I)}$.

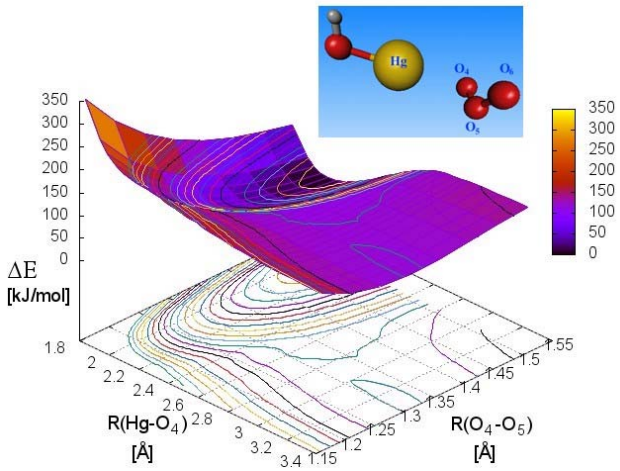

Figure 7. 3D scan of the PES in the close vicinity of the oxygen migration from O_3 to $HOHg^{(I)}$ at DK-CASPT2/ANO-RCC-VDZP level.

According to our calculations, NEVPT2, CAM-B3LYP-D3BJ, ωB97X-D3BJ, and BLYP energy profiles follow the same behavior as they do the oxidation of $BrHg^{(I)}$ (Figure S4 in Supp. Information). Therefore, we adopted the same methodology explained above. The FC is 52.1 and 38.8 kcal mol^{-1} lower than reactants at CCSD(T) and NEVPT2, respectively. This exit-channel complex, $HOHg^{(II)}O\text{-}O_2$, is formed following a barrierless ZPE-corrected energy profile, and after overcoming a barrier in the Gibbs free energy. Figure 8 displays the geometries of the variational TSs, the $TS_{min\text{-}min}$ and the FC. The Gibbs free energy barriers ($\Delta G^{\ddagger}$) range from 4.5 to 9.4 and 5.8 to 11.5 kcal mol^{-1} at CCSD(T) and NEVPT2 level, respectively (Figure 9). These free energy barriers are very similar to the ones obtained in the oxidation of $BrHg^{(I)}$. The calculated rate constants for R8 using MultiWell, are shown in Table S2 and Figure 10.

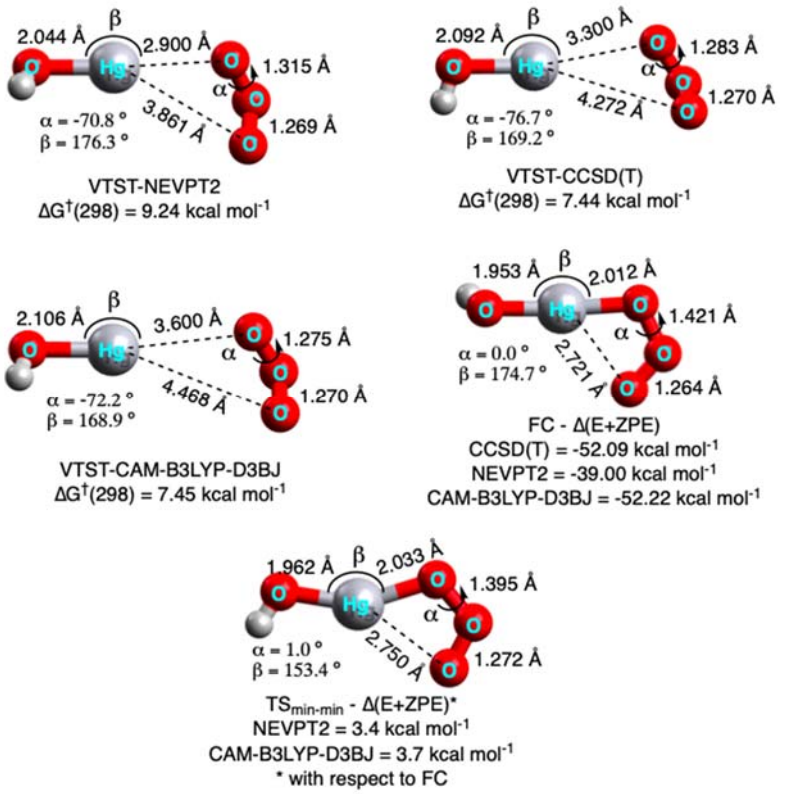

Figure 8. Variational TS, $TS_{min\text{-}min}$ and FC geometries for R8. Energies (in kcal mol^{-1}) at CCSD(T), NEVPT2, and CAM-B3LYP-D3BJ.

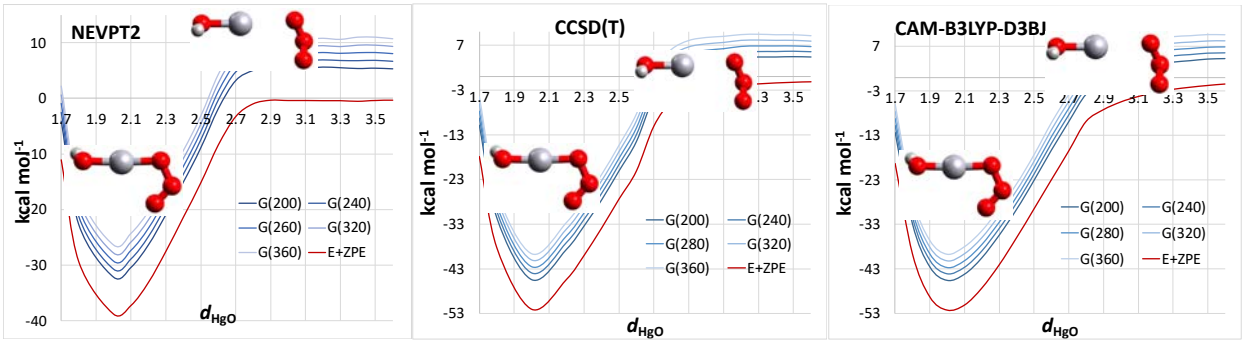

Figure 9. Energy profiles (kcal mol^{-1}) along the d_{HgO} distance for $HOHg^{(I)}$ oxidation. Energies have been calculated at High-Level using NEVPT2 and CCSD(T), taking as a reference the reactants separated at infinite distance and optimized at CAM-B3LYP-D3BJ. $G = E_{elec}^{High\text{-}Level} + G_{corr}^{DFT}$; $E = E_{elec}^{High\text{-}Level} + ZPE^{DFT}$.

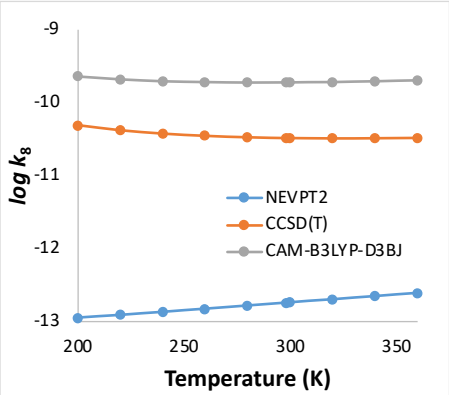

Figure 10. Logarithm of the variational TST rate constant k_8(T) (cm^3 $molecule^{-1}$ s^{-1}) for $HOHg^{(I)}$ oxidation as a function of the temperature according to CCSD(T), NEVPT2 and CAM-B3LYP-D3BJ energies.

Three sets of temperature dependent rate constants were calculated for R8 such as explained for R7. According to CAM-B3LYP-D3BJ, the rate constant for the oxidation of $HOHg^{(I)}$ with O_3 is three times faster than that for $BrHg^{(I)}$ oxidation at 298 K, but the CCSD(T) rate constant for $HOHg^{(I)}$ is about two times slower than the corresponding rate constant for $BrHg^{(I)}$. NEVPT2 gives rate constants about 200 times lower than the CCSD(T) rate constant, a much greater difference that was observed for $BrHg^{(I)}$ (factor of 14 error). Given the excellent performance of CCSD(T) and CAM-B3LYP-D3BJ for $BrHg^{(I)}$ oxidation by O_3, and their relatively good agreement for $HOHg^{(I)}$ oxidation by O_3, we conclude that NEVPT2 is failing for $HOHg^{(I)}$ oxidation by O_3. We further conclude the rate constants for oxidation of $BrHg^{(I)}$ and $HOHg^{(I)}$ by ozone possess fairly similar rate constants, and that the rate constant for $HOHg^{(I)}$ is likely closer to the experimental value for the analogous reaction of $BrHg^{(I)}$ than the value of 3.0×10^{-11} cm^3 $molecule^{-1}$ s^{-1} used in a recent modeling paper.[55]

The lowest energy species on the PES is the exit-channel complex HOHgOOO. This radical has two equivalent isomers analogously to $BrHg^{(I)}$, which are separated by a $TS_{min\text{-}min}$ that imposes a barrier of 3.7 kcal mol^{-1} at CAM-B3LYP-D3BJ (3.4 kcal mol^{-1} at NEVPT2). Separated products are 5.1 and 0.3 kcal mol^{-1} higher than the HOHgOOO exit-channel complexes at CCSD(T) and CAM-B3LYP-D3BJ, respectively. According to CAM-B3LYP-D3BJ, there is a barrier of 8.11 kcal mol^{-1} from the exit-channel to the final products. As with BrHgOOO, the chemically activated HOHgOOO will probably undergo prompt dissociation to separated reactants.

Reduction of BrHg by O_3

The reduction reaction is characterized by a reaction pathway involving a TS with d_{BrO} = 2.328 Å, weakened Br-Hg and O-O_2 bonds, whose d_{BrHg} and d_{OO} are 2.613 and 1.323 Å. The TS's imaginary frequency is -181 cm^{-1} and the displacement vector runs almost parallel to the axis formed by Br-O bond (Figure S8 in Supp. Information). The barrier imposed by the TS along the ZPE-corrected energy profile are 2.6 and 8.0 kcal mol^{-1} at CCSD(T) and NEVPT2, respectively, but barrierless at CAM-B3LYP-D3BJ and BLYP levels. At CAM-B3LYP-D3BJ level, the energy decreases 1.43 kcal mol^{-1} with respect to reactants separated at infinite distance, then the energy rises to the TS, which is -0.04 kcal mol^{-1}. This TS appears at CAM-B3LYP-D3BJ but not at BLYP level (Figure 11).

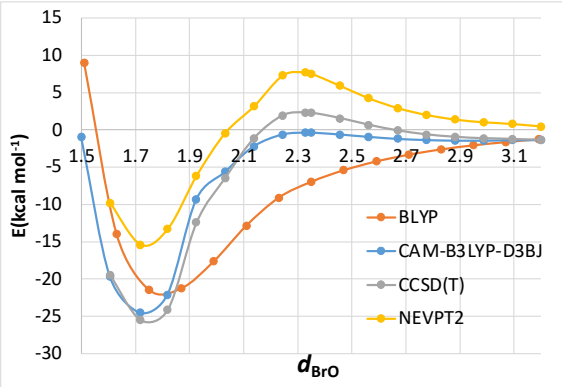

Figure 11. Energy profile obtained by relaxed scans at CAM-B3LYP-D3BJ and BLYP along the d_{BrO} for $BrHg^{(I)}$ reduction. CCSD(T) and NEVPT2 single points were carried out on the CAM-B3LYP-D3BJ geometries.

Once the barrier is overcome, an exit-channel complex (FC) is formed, which might be described as O_2—OBr—Hg, given that it is characterized by weak interactions between BrO, O_2 and Hg. This FC lies 26.1 and 16.0 kcal mol^{-1} lower than the reactants according to our CCSD(T) and NEVPT2 calculations, respectively. The Br-Hg bond is fully dissociated (d_{BrHg} = 3.5 Å vs 2.5 Å in $BrHg^{(I)}$) and the oxygen molecule in the FC remains over 3.6 Å from the BrO and Hg (Figure 12).

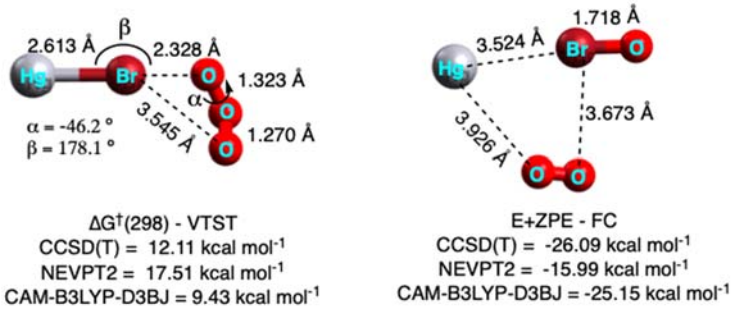

Figure 12. Variational TS and FC geometries for R9. Energies (in kcal mol^{-1}) at CCSD(T), NEVPT2, and CAM-B3LYP-D3BJ.

The Gibbs free energy profiles show maxima imposing barriers going from 8.7 to 14.3 kcal mol^{-1} at CCSD(T) (7.7 to 19.7 kcal mol^{-1} at NEVPT2 level) as the temperature increases from 200 to 360 K (Figure 13). The lower barriers were obtained with CAM-B3LYP-D3BJ, which are 6.0 and 11.6 kcal mol^{-1} at 200 K and 360 K, respectively. The predictions of the rate constants using MultiWell significantly differ from one method to the other, and they are shown in Table S3 (in Supp. Information) and Figure 14. Despite the large variation in computed rate constants for R9, all levels of theory predict that oxidation is much faster than reduction at all temperatures: by factors of about 10^3, 10^5, and 10^8 at 298 K for CAM-B3LYP-D3BJ, CCSD(T), and NEVPT2, respectively.

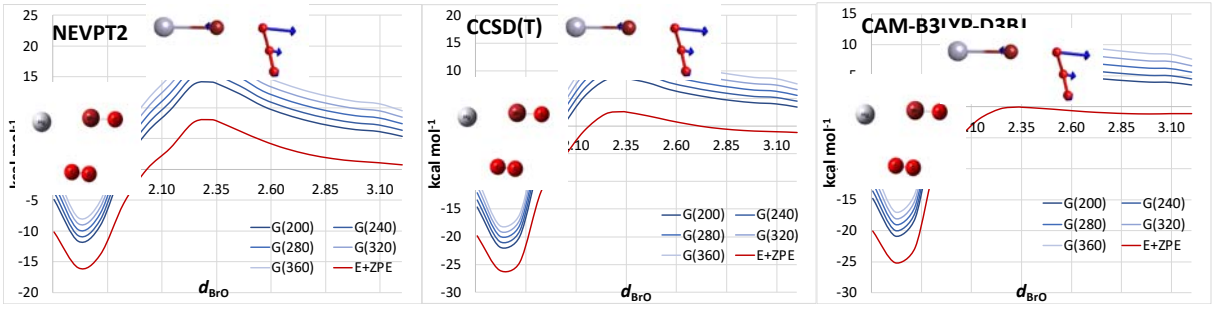

Figure 13. Energy profiles (kcal mol^{-1}) along the d_{BrO} distance for $BrHg^{(I)}$ reduction. Energies have been calculated at High-Level using NEVPT2 and CCSD(T), taking as a reference the reactants separated at infinite distance and optimized at CAM-B3LYP-D3BJ. $G = E_{elec}^{\text{High-Level}} + G_{corr}^{DFT}$; $E = E_{elec}^{\text{High-Level}} + ZPE^{DFT}$.

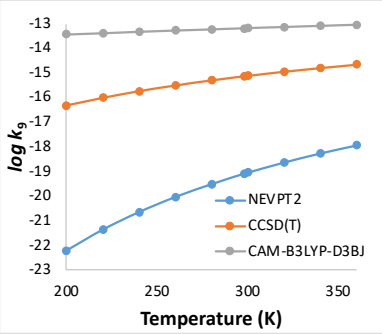

Figure 14. Logarithm of the variational TST rate constant k_9(T) (cm^3 $molecule^{-1}$ s^{-1}) as a function of the temperature according to CCSD(T), NEVPT2 and CAM-B3LYP-D3BJ energies.

The energy of the products separated at infinite distance is 2.0 and 2.4 kcal mol^{-1} higher than the exit-channel complex at CCSD(T) and CAM-B3LYP-D3BJ level, respectively. As with the final complexes from oxidation, we expect this complex to dissociate promptly; however, there is no reason to expect a saddle point for dissociation of this complex, give the large intermolecular distances shown in Figure 11.

Reduction of HOHg by O_3

The reduction reaction for $HOHg^{(I)}$ is analogue to the $BrHg^{(I)}$ one, thus, the TS along this reaction pathway has d_{HOO} = 1.847 Å and also weakened HO-Hg and O-O_2 bonds, with d_{HOHg} and d_{OO} equal to 2.319 and 1.333 Å, respectively (Figure 15). The TS's imaginary frequency is 508 cm^{-1} and the displacement vector is mostly composed by d_{HOO} (Figure S8 in Supp. Information). The calculated barriers imposed by the TS along the ZPE-corrected energy profiles are 11.5, 5.7 and 3.6 kcal mol^{-1} at NEVPT2, CCSD(T) and CAM-B3LYP-D3BJ, respectively. When the BLYP functional is used, the energy profile is barrierless (Figure 16).

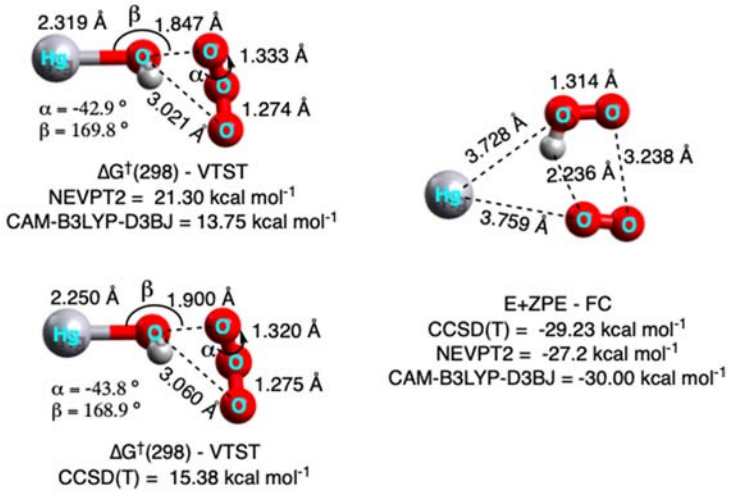

Figure 15. Variational TS and FC geometries for R9. Energies (in kcal mol^{-1}) at CCSD(T), NEVPT2, and CAM-B3LYP-D3BJ.

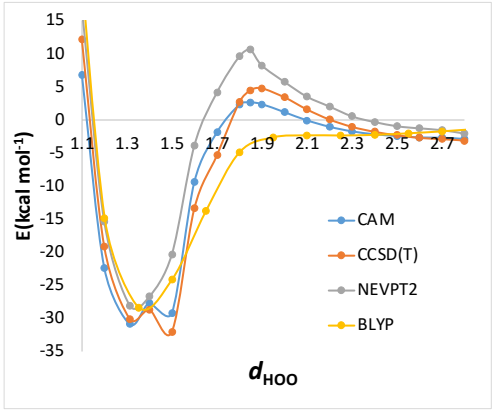

Figure 16. Energy profile obtained by relaxed scans at CAM-B3LYP-D3BJ and BLYP along the d_{HOO} for $HOHg^{(I)}$ reduction. CCSD(T) and NEVPT2 single points were carried out on the CAM-B3LYP-D3BJ geometries.

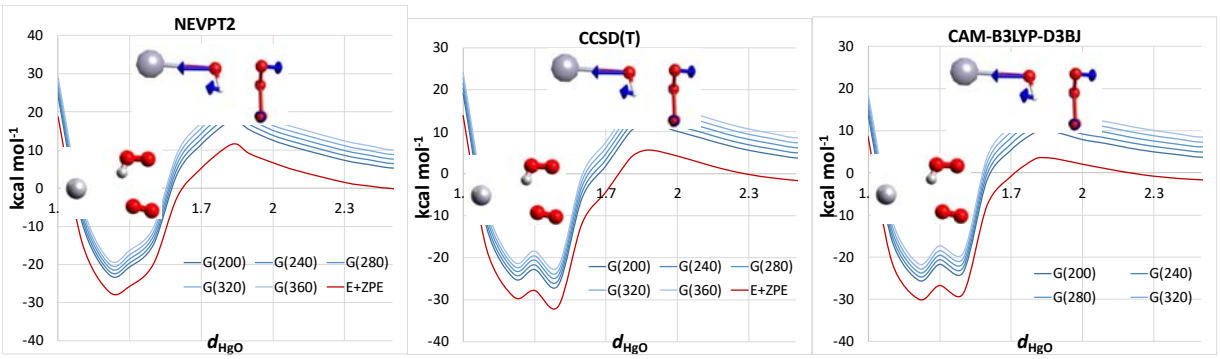

Figure 17. Energy profiles (kcal mol^{-1}) along the d_{HOO} distance for HOHg$^{(I)}$ reduction. Energies have been calculated at High-Level using NEVPT2 and CCSD(T), taking as a reference the reactants separated at infinite distance and optimized at CAM-B3LYP-D3BJ. $G = E_{elec}^{High\text{-}Level} + G_{corr}^{DFT}$; $E = E_{elec}^{High\text{-}Level} + ZPE^{DFT}$.

The Gibbs free energy profiles at 298 K show maxima imposing barriers of 15.3, 21.3 and 13.3 kcal mol^{-1} at CCSD(T), NEVPT2 and CAM-B3LYP-D3BJ level, respectively. The calculated rate constants are shown in Table S4 and Figure 18, and are at least a factor of one million lower than the rate constants for oxidation at all temperatures for each level of theory. The NEVPT2 and CCSD(T) rate constants at 298 K are lower than the CAM-B3LYP-D3BJ rate constant by factors of about 10^6 and 30, respectively. These discrepancies between levels of theory for this reduction reaction are a factor of ten larger than those we observed for BrHg$^{(I)}$ reduction.

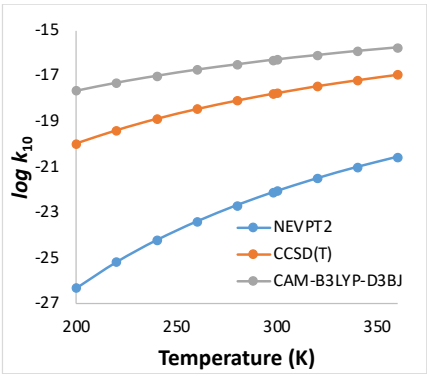

Figure 18. Logarithm of the variational TST rate constant k_{10}(T) (cm^3 molecule^{-1} s^{-1}) as a function of the temperature according to CCSD(T), NEVPT2 and CAM-B3LYP-D3BJ energies.

Once the barrier is overcome, an exit-channel complex is formed, which is ~30 kcal mol^{-1} lower than the reactants. This final complex is formed by weak interactions between HOO, O_2 and Hg (Figure 14).

Oddly, the products are 7.5 and 7.7 kcal mol^{-1} lower than the exit-channel complexes at CCSD(T) and CAM-B3LYP-D3BJ level, respectively. As with all the other final complexes, we expect this complex to dissociate promptly; like the O_2-BrO-Hg complex, we expect this complex to dissociate without a barrier.

Atmospheric Implications

This work confirms our preliminary results[55] indicating that $HOHg^{(I)}$ and $BrHg^{(I)}$ react with ozone with high rate constants to produce radical forms of $Hg^{(II)}$: $HOHg^{(II)}O$ and $BrHg^{(II)}O$, respectively. Our CCSD(T) and CAM-B3LYP-D3BJ values of k_7 at 298 K fall 13% above and 12% below, respectively, the recently obtained experimental value,[58] providing strong support for the validity of our computational approach. We predict a minimal temperature-dependence of this rate constant, which supports the reasonableness of the assumption of temperature independence made in two a recent modeling studies.[6,55]

The ratio of our CAM-B3LYP-D3BJ to CCSD(T) rate constants for $HOHg^{(I)} + O_3 \rightarrow HOHg^{(II)}O + O_2$ (R8) ranges from 4.7 to 6.1, but they nicely bracket the experimentally observed rate constant for $BrHg^{(I)} + O_3$. Consequently, the previous assumption, that k_8 equals k_7, appears reasonable.[55]

This paper presents the first study of the reduction channels in the reactions of $YHg^{(I)} + O_3$ (R9 and R10). Although the computed rate constants for these mercury reduction reactions depend more heavily on the computational approach than do k_8 and k_7, it is clear than the reduction reaction is utterly unimportant for $HOHg^{(I)}$, and very probably negligible for $BrHg^{(I)}$. If the rate constant, k_9, for reduction for $BrHg^{(I)}$ were to be non-negligible, it would interfere with the analysis of experimental data used by Gomez Martin et al. to determine k_7.[58]

The inclusion of R8 in a model of global mercury redox chemistry enormously increased the importance of OH-initiation oxidation of $Hg^{(0)}$to $Hg^{(II)}$, to the extent that ~40% of $HOHg^{(I)}$ was converted to $HOHg^{(II)}O$.[55] Because $BrHg^{(I)}$ is more stable than $HOHg^{(I)}$, close to 100% of it is converted to $BrHg^{(II)}O$. Consider then, what would result if one repeated that modeling but using

the experimental value of k_7, which is 2.4x higher than what the value that had been used. The extent (in Gg a^{-1}) of Br-initiated oxidation could scarcely increase, while the extent of OH-initiated oxidation would increase significantly. Given that the original study found that OH-initiation accounted for about 1/3 of total oxidation of $Hg^{(0)}$ to $Hg^{(II)}$, a revised study would likely find a much larger role for OH.

Since 2006,[13] modelers have been largely divided as to which of two competing mechanisms they used to account for GEM oxidation. Many modelers assume OH and O_3 can oxidize GEM to GOM in one step. Others have used the two-step model of Br-initiated oxidation put forth by Goodsite et al.[12] and first included in modeling by Holmes et al.[13] Subsequent comparisons of modeling results to field data made it hard to give up OH and/or O_3 as an oxidant in continental regions.[59-62] The present work shows that OH and O_3, together, not separately, can account for significant conversion of GEM to GOM.

CONCLUSIONS

The oxidation of $YHg^{(I)}$ is an obvious reaction for an atmospheric chemist to consider, as it a member of the large class of radical (R•) + ozone reactions:

$$R\bullet + O_3 \rightarrow RO + O_2 \qquad (R11)$$

Reaction of $BrHg^{(I)}$ and $HOHg^{(I)}$ been invoked in two modeling papers using estimated rate constants, and the rate constant for $BrHg^{(I)} + O_3$ was recently determined experimentally at room temperature. The reduction of $Hg^{(I)}$ to $Hg^{(0)}$ by reaction with ozone parallels the reduction of $BrHg^{(I)}$ in reactions with radicals (R2), reported from experiments[51,52] and computations.[49,51,108,109] This reduction of $HOHg^{(I)}$ by ozone proceeds about a million times slower than oxidation, whereas for $BrHg^{(I)}$ reduction is computed to be as much as 0.1% as fast as oxidation. The relatively greater feasibility of reduction for $BrHg^{(I)}$ than for $HOHg^{(I)}$ arises because both atoms of $BrHg^{(I)}$ possess comparable spin density, while the vast majority of the spin density of $HOHg^{(I)}$ resides on the Hg atom.[51]

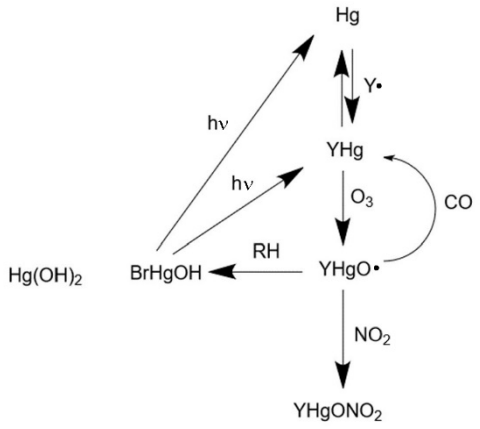

Scheme 1. Major reactions in redox cycling of $Hg^{(0)}$ in the gaseous atmosphere initiated by Y• = OH or Br. $Hg(OH)_2$ is not photolyzed in the troposphere.[110]

Scheme 1 provides an overview of the most important gas-phase reactions involved in mercury redox chemistry in the atmosphere. It illustrates the two-step mechanism for oxidation of $Hg^{(0)}$ to $Hg^{(II)}$, with ozone being the dominant species oxidizing $Hg^{(I)}$ intermediates. The rate constant for reduction of $BrHg^{(II)}O$ by CO is wildly uncertain,[111] and rate constants for reactions of $BrHg^{(II)}O$ + RH to form $BrHg^{(II)}OH$ have only been computed for RH = CH_4, C_2H_6, and $H_2C{=}O$;[19] we are drafting a manuscript showing that $HOHg^{(II)}O$ chemistry mimics $BrHg^{(II)}O$ chemistry. We are beginning to explore the reactions of $BrHg^{(II)}O$ and $HOHg^{(II)}O$ with ozone. Quantum yields of competing photolysis pathways of Br-containing $Hg^{(II)}$ species have only been computed in a single study at a single wavelength.[112] No experimental data exists for $HOHg^{(II)}O$, whatsoever, or for HOHg in the gas phase. Clearly, scientists must carry out more investigations of the physical chemistry of mercury before atmospheric modeling can provide reliable constraints on the global biogeochemical cycling of mercury.

ASSOCIATED CONTENT

Supporting Information

The Supporting Information is available free of charge.

AUTHOR INFORMATION

*** Corresponding Author**

Theodore S. Dibble - Department of Chemistry, State University of New York College of Environmental Science and Forestry, Syracuse, New York 13210, United States; orcid.org/0000-0002-0023-8233; Phone: (315) 470- 6596; Email: tsdibble@esf.edu

Authors

Pedro J. Castro − Department of Chemistry, State University of New York College of Environmental Science and Forestry, Syracuse, New York 13210, United States; orcid.org/0000-0003-1650-4708.

Vladimir Kellö − Department of Physical and Theoretical Chemistry, Faculty of Natural Sciences, Comenius University in Bratislava, 84215 Bratislava, Slovakia; orcid.org/0000-0003-2453-4296

Ivan Cernušák − Department of Physical and Theoretical Chemistry, Faculty of Natural Sciences, Comenius University in Bratislava, 84215 Bratislava, Slovakia; orcid.org/0000-0002-6597-3095;

Notes

The authors declare no competing financial interest.

ACKNOWLEDGEMENTS

This material is based upon work supported by the National Science Foundation under grant number 2004100 from the Chemistry Division of the U.S. National Science Foundation. IC and VK thank the Slovak Research and Development Agency for the support under the contract

APVV-20-0127 and the high-performance computing facility of the Centre for Information Technology (https://uniba.sk/en/HPC-Clara) at Comenius University.

REFERENCES

1. L. Si and P. A. Ariya, "*Recent Advances in Atmospheric Chemistry of Mercury"*. Atmosphere 2018, 9, 76.
2. P. Miretzky, A. F. Cirelli. "*Hg(II) removal from water by chitosan and chitosan derivatives: A review"*. J. Hazard. Mater. 2009, 167, 10–23.
3. N. Pirrone, R. Mason. "*Mercury fate and transport in the atmosphere: emissions, measurements and models"*. Springer, New York, 2009.
4. M. Subira, P. A. Ariyaa, A. P. Dastoor. "*A review of uncertainties in atmospheric modeling of mercury chemistry I. Uncertainties in existing kinetic parameters - Fundamental limitations and the importance of heterogeneous chemistry"*. Atmospheric Environment 45 (2011) 5664e5676.
5. AMAP/UN, Technical Background Report for the Global Mercury Assessment, "*2018. Arctic monitoring assessment programme Oslo, Norway/UN environment programme chemical health branch*". Switz, Geneva, 2019.
6. A. Saiz-Lopez, O. Travnikov, J. E. Sonke, C. P. Thackray, D. J. Jacob, J. Carmona-García, A. Francés-Monerrisf, D. Roca-Sanjuán, A. Ulises Acuña, J. Z. Dávalos, C. A. Cuevas, M. Jiskra, F. Wang, J. Bieser, J. M. C. Plane and J. S. Francisco. "*Photochemistry of oxidized Hg(I) and Hg(II) species suggests missing mercury oxidation in the troposphere"*. PNAS, 2020, 117 (49) 30949-30956.
7. N. Pirrone, K. R. Mahaffey. "*Dynamics of mercury pollution on regional and global scales: atmospheric processes and human exposures around the world"*. Springer, New York, 2005.
8. UNEP. "*Global Mercury Assessment 2013: Sources, Emissions, Releases, and Environmental Transport"*; UNEP Chemicals Branch: Geneva, Switzerland, 2013.
9. D. Obrist et al., "*A review of global environmental mercury processes in response to human and natural perturbations: Changes of emissions, climate, and land use"*. Ambio 47, 116–140 (2018).

10. P. A. Ariya, M. Amyot, A. Dastoor, D. Deeds, A. Feinberg, G. Kos, A. Poulain, A. Ryjkov, K. Semeniuk, M. Subir, K. Toyota. "*Mercury physicochemical and biogeochemical transformation in the atmosphere and at atmospheric interfaces: A review and future directions"*. Chem. Rev., 2015, 115, 3760–3802.
11. H. M. Horowitz et al., "*A new mechanism for atmospheric mercury redox chemistry: Implications for the global mercury budget"*. Atmos. Chem. Phys. 2017, 17, 6353–6371.
12. M. E. Goodsite, J. M. C. Plane, H. Skov, "*A theoretical study of the oxidation of Hg^0 to $HgBr_2$ in the troposphere".* Environ. Sci. Technol. 38, 1772–1776 (2004).
13. C. D. Holmes, D. J. Jacob, X. Yang, "*Global lifetime of elemental mercury against oxidation by atomic bromine in the free troposphere"*. Geophys. Res. Lett. 2006, 33, L20808.
14. F. Wang et al., "*Enhanced production of oxidised mercury over the tropical Pacific Ocean: A key missing oxidation pathway".* Atmos. Chem. Phys. 2014, 14, 1323–1335.
15. C. D. Holmes et al., "*Global atmospheric model for mercury including oxidation by bromine atoms"*. Atmos. Chem. Phys. 2010, 10, 12037–12057.
16. T. S. Dibble, A. C. Schwid, "*Thermodynamics limits the reactivity of BrHg radical with volatile organic compounds".* Chem. Phys. Lett. 2016, 659, 289–294.
17. T. S. Dibble, M. Zelie, H. Mao. "*Thermodynamics of reactions of ClHg and BrHg radicals with atmospherically abundant free radicals*." Atmos. Chem. Phys. 2012, 12, 10271–10279.
18. Y. Jiao, T. S. Dibble. "*First kinetic study of the atmospherically important reactions BrHg+ NO_2 and BrHg+ HOO"*. Phys. Chem. Chem. Phys. 2017, 19, 1826–1838.
19. T. S. Dibble, H. L. Tetu, Y. Jiao, C. P. Thackray, D. J. Jacob. "*Modeling the OH-initiated oxidation of mercury in the global atmosphere without violating physical laws"*. J. Phys. Chem. A, 2020, 124, 444–453.
20. C. T. Driscoll, R. P. Mason, H. M. Chan, D. J. Jacob, N. Pirrone, N. "*Mercury as a Global Pollutant: Sources, Pathways, and Effects"*. Environ. Sci. Technol. 2013, 47, 4967−4983.
21. W. H. Schroeder, J. Munthe. "*Atmospheric mercury-An overview"*. Atmos. Environ. 1998, 32, 809−822.

22. C. J. Lin, P. Pongprueksa, O. Russell Bullock, S. E. Lindberg, S. O. Pehkonen, C. Jang, T. Braverman, T. C. Ho. "*Scientific Uncertainties in Atmospheric Mercury Models II: Sensitivity Analysis in the CONUS Domain"*. Atmos. Environ. 2007, 41, 6544−6560.
23. J. Zhou and D. Obrist, "*Global Mercury Assimilation by Vegetation*". Environ. Sci. Technol. 2021, 55, 20, 14245–14257.
24. C. R. Hammerschmidt, W. F. Fitzgerald. "*Methylmercury in freshwater fish linked to atmospheric mercury deposition"*. Environ. Sci. Technol. 2006, 40, 7764–7770.
25. A. R. Schwindt, J. W. Fournie, D. H. Landers, C. B. Schreck, M. L. Kent. "*Mercury concentrations in salmouids from western US National Parks and relationships with age and macrophage aggregates"*. Environ. Sci. Technol. 2008, 42, 1365–1370.
26. J. R. Barrett. "*Rice is a significant source of methylmercury: research in China assesses exposures".* Environ. Health Perspect. 2010, A398.
27. P. Li, X. Feng, G. Qiu. "*Methylmercury exposure and health effects from rice and fish consumption: a review"*. Int. J. Environ. Res. Public Health, 2010, 7, 2666–2691.
28. P. Li, X. Feng, X. Yuan, H. M. Chan, G. Qiu, G. X. Sun, Y. G. Zhu. "*Rice consumption contributes to low level methylmercury exposure in southern China".* Environ. Int. 2012, 49, 18–23.
29. H. Zhang, X. Feng, T. Larssen, G. Qiu, R. D. Vogt. "*In inland China, rice, rather than fish, is the major pathway for methylmercury exposure".* Environ. Health Perspect. 2010, 118, 1183–1188.
30. H. Zhao, H. Yan, L. Zhang, G. Sun, P. Li, X. Feng. "*Mercury contents in rice and potential health risks across China".* Environ. Int. 2019, 126, 406–412.
31. A. Saiz-Lopez, S. P. Sitkiewicz, D. Roca-Sanjuán, J. M. Oliva-Enrich, J. Z. Dávalos, R. Notario, M. Jiskra, Y. Xu, F. Wang, C. P. Thackray, E. M. Sunderland, D. J. Jacob, O. Travnikov, C. A. Cuevas, A. U. Acuña, D. Rivero, J. M. C. Plane, D. E. Kinnison, J. E. Sonke "*Photoreduction of gaseous oxidized mercury changes global atmospheric mercury speciation, transport and deposition"*. Nat. Commun. 2018, 9, 4796.
32. B. Hall. "*The gas phase oxidation of elemental mercury by ozone*". 1995, Water, Air, and Soil Pollution, 80, 301-315.
33. B. Pal and P. A. Ariya. "*Studies of ozone-initiated reactions of gaseous mercury: kinetics, product studies, and atmospheric implications*". 2004, 6, 572-579.

34. A. L. Summer, C. Spicer, K. A. Cowen, M. S. Landis. "*Environmental Chamber Studies of Mercury Reactions in the Atmosphere*". Dynamics of Mercury Pollution on Regional and Global Scales: Chapter 9. 2005, 10.1007/0-387-24494-8_9.
35. A. P. Ruttera, K. M. Shakya, R. Lehr, J. J. Schauer, R. J. Griffin. "*Oxidation of gaseous elemental mercury in the presence of secondary organic aerosols*". 2012, 59, 86-92.
36. J. G. Calvert, S. E. Lindberg. "*Mechanisms of mercury removal by O3 and OH in the atmosphere*" Atmos. Environ. 2005, 39, 3355 – 3367.
37. A. J. Hynes, D. L. Donohoue, M. E. Goodsite, I. M. Hedgecock. "*Our Current Understanding of Major Chemical and Physical Processes Affecting Mercury Dynamics in the Atmosphere and at the Air-Water/Terrestrial Interfaces".* Mercury Fate and Transport in the Global Atmosphere, Springer US, Boston, 2009, pp. 427 – 457.
38. C. D. Holmes, D. J. Jacob, X. Yang. "*Global lifetime of elemental mercury against oxidation by atomic bromine in the free troposphere*". Geophys. Res. Lett. 2006, 33, L20808.
39. J. A. Tossell. "*Calculation of the Energetics for Oxidation of Gas-Phase Elemental Hg by Br and BrO".* J. Phys. Chem. A, 2003, 107 (39), 7804−7808.
40. B. C. Shepler, N. B. Balabanov, K. A. Peterson. "*Ab Initio Thermochemistry Involving Heavy Atoms: An Investigation of the Reactions Hg + IX (X = I, Br, Cl, O)*". J. Phys. Chem. A, 2005, 109, 45, 10363-10372.
41. D. Cremer, E. Kraka, M. Filatov. "*Bonding in Mercury Molecules Described by the Normalized Elimination of the Small Component and Coupled Cluster Theory*". Chem. Phys. Chem. 2008, 9(17), 2510-2521.
42. J. Liu, W. Qu, J. Yuan, S. Wang, J. Qiu, and C. Zheng. "*Theoretical Studies of Properties and Reactions Involving Mercury Species Present in Combustion Flue Gases*". Energy Fuels 2010, 24, 1, 117-122.
43. J. Wilcox, D. C. J. Marsden, P. Blowers. "*Evaluation of basis sets and theoretical methods for estimating rate constants of mercury oxidation reactions involving chlorine*". Fuel Processing Technology, 2004, 85(5), 391-400.
44. A. Saiz-Lopez, R. von Glasow. "*Reactive halogen chemistry in the troposphere*". Chem. Soc. Rev. 41, 6448–6472 (2012).

45. W. R. Simpson, S. S. Brown, A. Saiz-Lopez, J. A. Thornton, Rv. Glasow. "*Tropospheric Halogen Chemistry: Sources, Cycling, and Impacts*". Chem. Rev. 2015, 115, 4035–4062.
46. P. A. Ariya, A. Khalizov, A. Gidas. "*Reactions of Gaseous Mercury with Atomic and Molecular Halogens: Kinetics, Product Studies, and Atmospheric Implications"*. J. Phys. Chem. A 2002, 106 (32), 7310−7320.
47. D. L. Donohoue, D. Bauer, B. Cossairt, A. J. Hynes. "*Temperature and Pressure Dependent Rate Coefficients for the Reaction of Hg with Br and the Reaction of Br with Br: A Pulsed Laser Photolysis-Pulsed Laser Induced Fluorescence Study"*. J. Phys. Chem. A, 2006, 110 (21), 6623−6632.
48. G. Sun, J. Sommar, X. Feng, C-J. Lin, M. Ge, W. Wang, R. Yin, X. Fu, L. Shang. "*Mass-Dependent and -Independent Fractionation of Mercury Isotope during Gas-Phase Oxidation of Elemental Mercury Vapor by Atomic Cl and Br*". Environ. Sci. Technol. 2016, 50, 17, 9232–9241.
49. N. B. Balabanov, B. C. Shepler, K. A. Peterson. "*Accurate Global Potential Energy Surface and Reaction Dynamics for the Ground State of $HgBr_2$"*. J. Phys. Chem. A, 2005, 109 (39), 8765−8773.
50. M. E. Goodsite, J. M. C. Plane, H. Skov. "*Correction to A Theoretical Study of the Oxidation of Hg^0 to $HgBr_2$ in the Troposphere"*. Environ. Sci. Technol. 2012, 46 (9), 5262−5262.
51. R. Wu, P. J. Castro, C. Gaito, K. Beiter, T. S. Dibble, and C. Wang "*Combined Experimental and Computational Kinetics Studies for the Atmospherically Important BrHg Radical Reacting with NO and O_2*". J. Phys. Chem. A 2022, Article ASAP. DOI: 10.1021/acs.jpca.2c02531.
52. R. Wu, C. Wang, T. S. Dibble. "*First experimental kinetic study of the atmospherically important reaction of BrHg + NO_2*". Chem. Phys. Lett. 2020, 759, 137928.
53. J. Sommar, K. Gaŕdfeldt, D. Strömberg, X. Feng. "*A Kinetic Study of the Gas-Phase Reaction Between the Hydroxyl Radical and Atomic Mercury".* Atmos. Environ. 2001, 35 (17), 3049−3054.
54. B. Pal, P. A. Ariya. "*Gas-Phase HO•-Initiated Reactions of Elemental Mercury: Kinetics, Product Studies, and Atmospheric Implications"*. Environ. Sci. Technol. 2004, 38 (21), 5555−5566.

55. V. Shah, D. J. Jacob, C. P. Thackray, X. Wang, E. M. Sunderland, T. S. Dibble, A. Saiz-Lopez, I. Černusǎk, V. Kellö, P. J. Castro, R. Wu, and C. Wang. "*Improved Mechanistic Model of the Atmospheric Redox Chemistry of Mercury"*. Environ. Sci. Technol. 2021, 55, 14445−14456.
56. J. Calvert, S. Lindberg. "*Mechanisms of Mercury Removal by O_3 and OH in the Atmosphere".* Atmos. Environ. 2005, 39 (18), 3355− 3367.
57. K. Lam. "*Chemistry and Implications of a Previously-Unknown Intermediate in the Atmospheric Mercury Oxidation*". 2019, State University of New York, College of Environmental Science and Forestry, ProQuest Dissertations Publishing, 29073743.
58. J. C. Gómez Martín, T. R. Lewis, K. M. Douglas, M.A. Blitz, A. Saiz-Lopez, J. M. C. Plane. "*The reaction between HgBr and O_3: kinetic study and atmospheric implications*". Phys. Chem. Chem. Phys. 2022, 24, 12419-12432.
59. M. Gabay, S. Raveh-Rubin, M. Peleg, E. Fredj and E. Tas. "*Is oxidation of atmospheric mercury controlled by different mechanisms in the polluted continental boundary layer vs. remote marine boundary layer?*". Environ. Res. Lett. 2020, 15, 064026.
60. Z. Ye, H. Mao, C-J. Lin, S. Y. Kim. "*Investigation of processes controlling summertime gaseous elemental mercury oxidation at midlatitudinal marine, coastal, and inland sites*". Atmos. Chem. Phys. 2016, 16, 8461-8478. P.
61. Weiss-Penzias, H. M. Amos, N. E. Selin, M. S. Gustin, D. A. Jaffe, D. Obrist, G.-R. Sheu, A. Giang. "*Use of a global model to understand speciated atmospheric mercury observations at five high-elevation sites*". Atmos. Chem. Phys. 2015, 15, 1161-1173.
62. I. Cheng, L. Zhang, H. Mao, Z. Ye, R. Keenan. "*Atmospheric Chemistry of Gaseous Oxidized Mercury at a Coastal Site in Atlantic Canada*". J. Atmos. Scien. 2020, 77(3), 1137-1149.
63. Neese, F. "*The ORCA program system*" Wiley interdisciplinary Reviews - Computational Molecular Science, 2012, 2(1), 73-78.
64. M. J. Frisch, G. W. Trucks, H. B. Schlegel, G. E. Scuseria, M. A. Robb, J. R. Cheeseman, G. Scalmani, V. Barone, G. A. Petersson, H. Nakatsuji et al. *Gaussian 16*, Revision A.01, Gaussian Inc.: Wallingford CT, 2016.
65. T. H. Dunning Jr. "*Gaussian basis sets for use in correlated molecular calculations. I. The atoms boron through neon and hydrogen"*. J. Chem. Phys. 1989, 90, 1007.

66. K. A. Peterson, D. E. Woon, T. H. Dunning, Jr. "*Benchmark calculations with correlated molecular wave functions. IV. The classical barrier height of the H+H$_2$ →H$_2$+H reaction*". J. Chem. Phys. 1994, 100 (10), 7410-7415.

67. K. A. Peterson, C. Puzzarini. *"Systematically convergent basis sets for transition metals. II. Pseudopotential-based correlation consistent basis sets for the group 11 (Cu, Ag, Au) and 12 (Zn, Cd, Hg) elements"*. Theor. Chem. Acc. 2005, 114, 283.

68. K.A. Peterson, D. Figgen, E. Goll, H. Stoll, M. Dolg. "*Systematically convergent basis sets with relativistic pseudopotentials. II. Small-core pseudopotentials and correlation consistent basis sets for the post-d group 16-18 elements".* J. Chem. Phys. 2003, 119, 11113.

69. D. Figgen, G. Rauhut, M. Dolg, H. Stoll. "*Energy-consistent pseudopotentials for group 11 and 12 atoms: adjustment to multi-configuration Dirac–Hartree–Fock data"*. Chem. Phys. 2005, 311, 227.

70. C. Moller and M. S. Plesset. "*Note on an Approximation Treatment for Many-Electron Systems*". Physical Review. 1934, 46, 618-622.

71. A. D. Becke, "*Density-Functional Thermochemistry. V. Systematic Optimization of Exchange-Correlation Functionals*". J. Chem. Phys. 1997, *107*, 8554-8560.

72. S. Grimme, S Ehrlich, L. Goerigk. "*Effect of the Damping Function in Dispersion Corrected Density Functional Theory*". J. Comp. Chem. 2011, *32*, 1456-1465.

73. A. D. Becke, "*Density-functional exchange-energy approximation with correct asymptotic-behavior*" Phys. Rev. A, 1988, 38, 3098-100.

74. B. Miehlich, A. Savin, H. Stoll, H. Preuss. "*Results obtained with the correlation-energy density functionals of Becke and Lee, Yang and Parr*" Chem. Phys. Lett. 1989, 157, 200-206.

75. B. O. Roos, "*The Complete Active Space Self-Consistent Field Method and Its Applications in Electronic Structure Calculations*". Adv. Chem. Phys. 1987, *69*, 399.

76. K. Andersson, P. A. Malmqvist, B. O. Roos, K. Wolinski. "*Second-order perturbation theory with a CASSCF reference function*". J. Phys. Chem. 1990, 94(14), 5483.

77. K. Andersson, P. A. Malmqvist, B. O. Roos. "*Second-order perturbation theory with a complete active space self-consistent field reference function*" J. Chem. Phys. 1992, 96, 1218.

78. C. Angeli, R. Cimiraglia, S. Evangelisti, T. Leininger, J.-P. Malrieu. "*Introduction of n-Electron Valence States for Multireference Perturbation Theory*". J. Chem. Phys. 2001, *114*, 10252.

79. C. Angeli, R. Cimiraglia, J.-P. Malrieu. "*N-Electron Valence State Perturbation Theory: A Fast Implementation of the Strongly Contracted Variant*". Chem. Phys. Lett. 2001, *350*, 297-305.

80. C. Angeli, R. Cimiraglia, J.-P. Malrieu. "*N-Electron Valence State Perturbation Theory: A Spinless Formulation and an Efficient Implementation of the Strongly Contracted and of the Partially Contracted Variants*". J. Chem. Phys. 2002, *117*, 9138.

81. I. Schapiro, K. Sivalingam, F. Neese. "*Assessment of N-Electron Valence State Perturbation Theory for Vertical Excitation Energies*". J. Chem. Theory Comput. 2013, *9*, 3567–3580.

82. C. Angeli, S. Borini, M. Cestari, R. Cimiraglia. "*A Quasidegenerate Formulation of the Second Order N-Electron Valence State Perturbation Theory Approach*". *J. Chem. Phys.* 2004, 121, 4043.

83. P. G. Szalay, T. Muller, H. Lischka. "*Excitation energies and transition moments by the multireference averaged quadratic coupled cluster (MR-AQCC) method*". Phys. Chem. Chem. Phys. 2000, 2, 2067-2073.

84. P. Piecuch, M. Włoch. "*Renormalized coupled-cluster methods exploiting left eigenstates of the similarity-transformed Hamiltonian*". J. Chem. Phys. 2005, 123, 224105.

85. M. Esser. "*Direct MRCI method for the calculation of relativistic many-electron wavefunctions. I. General formalism*". Int. J. Quantum Chem. 1984, 26(3), 313-338.

86. L. Meisser. "*Size-consistency corrections for configuration interaction calculations*". Chem. Phys. Lett. 1988, 146(3-4), 204-210.

87. F. Aquilante, J. Autschbach, R. K. Carlson, L. F. Chibotaru, M. G. Delcey, L. De Vico, I. Fdez. Galván, N. Ferré, L. M. Frutos, L. Gagliardi, M. Garavelli, A. Giussani, C. E. Hoyer, G. Li Manni, H. Lischka, D. Ma, P. Å. Malmqvist, T. Müller, A. Nenov, M. Olivucci, T. B. Pedersen, D. Peng, F. Plasser, B. Pritchard, M. Reiher, I. Rivalta, I. Schapiro, J. Segarra-Martí, M. Stenrup, D. G. Truhlar, L. Ungur, A. Valentini, S. Vancoillie, V. Veryazov, V. P. Vysotskiy, O. Weingart, F. Zapata, R. Lindh, Journal of Computational Chemistry, 2016, 37, 506.

88. M. Douglas and N. M. Kroll. "*Quantum electrodynamical corrections to the fine structure of helium*". Ann. Phys. 1974, 82, 89-155.
89. B. A. Hess. "*Relativistic electronic-structure calculations employing a two-component no-pair formalism with external-field projection operators*". Phys. Rev. A,1986, 33, 3742-3748.
90. B. O. Roos, R. Lindh, P-Å. Malmqvist, V. Veryazov, P-O. Widmark. "*Main group atoms and dimers studied with a new relativistic ANO basis set*". J. Phys. Chem. A, 2004, 108, 2851-2858.
91. B. O. Roos, R. Lindh, P-Å. Malmqvist, V. Veryazov, and P-O. Widmark. "*New relativistic ANO basis sets for transition metal atoms*". J. Phys. Chem. A, 2005, 109, 6575-6579
92. T. Yanai, D. P Tew, N. C. Handy. "*A new hybrid exchange–correlation functional using the Coulomb-attenuating method (CAM-B3LYP)*" Chem. Phys. Lett. 2004, 393(1-3), 51-57.
93. J.-D. Chai, M. Head-Gordon, "*Systematic optimization of long-range corrected hybrid density functionals*" *J. Chem. Phys.* 2008, 128, 084106.
94. S. Grimme, S. Ehrlich, L. Goerigk. "*Effect of the damping function in dispersion corrected density functional theory*" J. Comput. Chem. 2011, 32, 1456–1465.
95. S. Grimme, J. Antony, S. Ehrlich, H. Krieg. "*A consistent and accurate ab initio parametrization of density functional dispersion correction (DFT-D) for the 94 elements H-Pu*", J. Chem. Phys. 2010, 132, 154104.
96. G. D. III Purvis, R. J. Bartlett. "*A Full Coupled-Cluster Singles and Doubles Model: The Inclusion of Disconnected Triples*". J. Chem. Phys. 1982, 76, 1910-1918.
97. J. A. Pople, M. Head-Gordon, K. Raghavachari. "*Quadratic Configuration Interaction. A General Technique for Determining Electron Correlation Energies*". J. Chem. Phys. 1987, 87, 5968-5975.
98. J. R. Barker, T. L. Nguyen, J. F. Stanton, C. Aieta, M. Ceotto, F. Gabas, T. J. D. Kumar, C. G. L. Li, L. L. Lohr, A. Maranzana, et al. "*MultiWell-2021 Software Suite"*, University of Michigan: Ann Arbor, Michigan, USA, 2021. https://multiwell.engin.umich.edu/.
99. J. R. Barker. "*Multiple-Well, Multiple-Path Unimolecular Reaction Systems. I. MultiWell Computer Program Suite*". Int. J. Chem. Kinetics 2001, 33, 232-245.

100. J. R. Barker. "*Energy Transfer in Master Equation Simulations: A New Approach*". Int. J. Chem. Kinetics 2009, 41, 748-763.
101. S. D. Le Picard, M. Tizniti, A. Canosa. I. R. Sims, I. W. M. Smith. "*The Thermodynamics of the Elusive HO_3 Radical*". Science, 2010, 328 (5983), 1258-1262.
102. J. M. Anglada, S. Olivella and A. Solé. "*On the Dissociation of Ground State trans-HOOO Radical: A Theoretical Study*". J. Chem. Theory Comput. 2010, 6, 9, 2743–2750.
103. NIST Computational Chemistry Comparison and Benchmark Database. NIST Standard Reference. Database Number 101. Release 22, May 2022, Editor: Russell D. Johnson III. http://cccbdb.nist.gov/ DOI:10.18434/T47C7Z.
104. K. Sumayo S. Sumiyoshi Y. Endo. "*The Rotational Spectrum and Structure of the HOOO Radical*". Science, 2005, 308(5730), 1885-1886.
105. M. E. Varner, M. E. Harding, J. Vázquez, J. Gauss, J. F. Stanton. "*Dissociation Energy of the HOOO Radical*". J. Phys. Chem. A 2009, 113, 42, 11238–11241.
106. R. P. Fernandez, R. J. Salawitch, D. E. Kinnison, J.-F. Lamarque, A. Saiz-Lopez. "*Bromine Partitioning in the Tropical Tropopause Layer: Implications for Stratospheric Injection*". Atmos. Chem. Phys. 2014, 14 (24), 13391-13410.
107. A. Saiz-Lopez, R. P. Fernandez. "*On the Formation of Tropical Rings of Atomic Halogens: Causes and Implications*". Geophys. Res. Lett. 2016, 43 (6), 2928-2935.
108. J. Wilcox and T. Okano. "*Ab initio-based Mercury Oxidation Kinetics via Bromine at Postcombustion Flue Gas Conditions*". Energy Fuels, 2011, 25, 4, 1348–1356.
109. Y. Jiao, T. S. Dibble. "*Structures, Vibrational Frequencies, and Bond Energies of the BrHgOX and BrHgXO Species Formed in Atmospheric Mercury Depletion Events*". J Phys Chem A. 2017, 121(41), 7976-7985.
110. D. Strömberg, O. Gropen, U. Wahlgren. "*Non-relativistic and relativistic calculations on some Zn, Cd and Hg complexes*". Chem. Phys. 1989, 133(2), 207-219.
111. D. Khiri, F. Louis, I. Černušák, Theodore S. Dibble. "*BrHgO• + CO: Analogue of OH + CO and Reduction Path for Hg(II) in the Atmosphere*". ACS Earth Space Chem. 2020, 4, 10, 1777-1784.
112. A. Francés-Monerris, J. Carmona-García, A. U. Acuña, J. Z. Dávalos, C. A. Cuevas, D. E. Kinnison, J. S. Francisco, A. Saiz-Lopez, D. Roca-Sanjuán. "*Photodissociation*

Mechanisms of Major Mercury(II) Species in the Atmospheric Chemical Cycle of Mercury". Angewandte Chem. 2019, 59(19), 7605-7610